Polymer Journal
https://doi.org/10.1038/s41428-020-00428-0

ORIGINAL ARTICLE

Recyclable liquid crystal polymeric sensor beads based on the assistance of radially aligned liquid crystals

Jui-Hsiang Liu[1] · Yi-Hua Hung[1] · Ssu-Ni Lin[1] · Sergey A. Shvetsov[2,3] · Vladimir Yu. Rudyak[2] · Alexander V. Emelyanenko[2] · Chun-Yen Liu[4]

Received: 21 July 2020 / Accepted: 7 September 2020

Abstract

In this study, we first demonstrate the synthesis of recyclable polymer beads for Cu^{2+} sensing based on radially aligned liquid crystal (LC) assistance. To detect metal ions in water, sensing probe monomers and polymers derived from rhodamine B were synthesized. Recyclable polymeric LC beads were prepared from LC monomers RM257 and RM105, a nonreactive mesogen of 5CB and a rhodamine B-derived monomer. Due to the assistance of radially aligned LCs, highly sterically hindered spirocyclic terminal groups of rhodamine B-derived monomers were aligned and fixed at the outer surface of liquid crystal beads. The color of the polymeric LC beads changed from light pink to deep pink after the beads were dropped into an aqueous Cu^{2+} solution. The results were ascribed to the spiro ring-opening mechanism. The addition of a nonreactive mesogen resulted in the porous structure of the polymeric LC beads. The high sensitivity of the Cu^{2+} solution using polymeric LC beads was confirmed. The fabricated polymeric LC beads were recycled by putting the polymeric LC beads into aqueous ammonia. The removal of Cu^{2+} from polymeric LC beads was due to the formation of $[Cu(NH_3)_4]^{2+}$. This recyclable LC bead sensor is an easy method for the detection of metal ions in aqueous solutions.

Introduction

The typical techniques used for quantitative analysis of metal ions are inductively coupled plasma-mass spectrometry, inductively coupled plasma with atomic emission spectroscopy, chromatography, atomic absorption spectrometry, neutron activation analysis, etc. Disappointingly, these methods require extensive sample preparation steps, high-cost instruments, and well-trained individuals and operations. Therefore, over the past few decades, many convenient sensors have been developed to detect different heavy metal ions [1–7]. Due to biomagnification, heavy metals will eventually enter the human body at high concentrations and cause damage to organs and body functions [8–10]. For instance, copper is necessary for health, but high concentrations of copper are harmful. Inhalation of high concentrations of copper can cause nose and throat irritation [11–14]. Ingestion of high concentrations of copper can cause damage to the liver and kidneys [15–17].

It is well known that liquid crystal (LC) molecules are sensitive to external stimuli from the surroundings, such as electric fields, magnetic fields, temperature, UV–vis light, and stress [18–23]. Radial alignment of LCs was achieved and studied using polarized optical microscopy (POM) [24–26]. On the other hand, rhodamine-based sensors have attracted great attention and have been widely developed in several research field due to their application potential and excellent photophysical properties, such as their great photostability, great quantum yield, specific color response, and relatively long emission wavelengths in the visible region. Rhodamine-based sensors are known for the detection of metal ions,

Supplementary information The online version of this article (https://doi.org/10.1038/s41428-020-00428-0) contains supplementary material, which is available to authorized users.

✉ Chun-Yen Liu
cyliu@gs.ncku.edu.tw

[1] Department of Chemical Engineering, National Cheng Kung University, No. 1, University Road, East Dist., Tainan City 70101, Taiwan

[2] Department of Physics, Lomonosov Moscow State University, Leninskie Gory, GSP-1, Moscow, Russia119991

[3] Lebedev Physical Institute, Leninsky pr. 53, Moscow, Russia119991

[4] Department of Materials Science and Engineering, National Cheng Kung University, No. 1, University Road, East Dist., Tainan City 70101, Taiwan

Published online: 15 October 2020

including Fe^{3+}, Cu^{2+}, Zn^{2+}, Al^{3+}, Cr^{3+}, Hg^{2+}, Au^{3+}, Pb^{2+}, and Pd^{2+}, in aqueous solutions and living cells via the ring-open reaction of the spirolactam structure after coordinating with anions or metal ions [27–32].

Singh et al. synthesized amphiphilic MeDTC-doped 5CB LC for a real-time detection method of Hg^{2+} ions in water [33]. LC molecules aligned at the aqueous interface, and polar head group of the amphiphile acted as mercuric ion-specific chelating ligands. Jang et al. demonstrated a simple, sensitive, and rapid label-free detection method for heavy metal ions using LC droplet patterns on a solid surface [34]. Xu et al. synthesized a new rhodamine B derivative colorimetric and fluorescence sensor by the condensation reaction of rhodamine B hydrazide and 2,4-dihydroxybenzaldehyde. The sensor had outstanding sensitive and selective recognition toward Cu^{2+} over the other examined metal ions [35, 36].

In our previous review paper, many papers published chemosensors with low-molecular-weight rhodamine B derivatives as well as recyclable beads immobilized on gold, silver, alginate gel, and latex beads [37–41]. Rhodamine B is a well-known material for sensing heavy metal ions. LC beads show a highly ordered radial arrangement in aqueous solutions. However, modification of highly ordered LC bead surfaces via rhodamine B derivatives for metal ion sensor design has not been shown in previously reported papers. In this study, we first demonstrated the synthesis of recyclable polymer beads for Cu^{2+} sensing via radially aligned LC assistance. To use highly ordered LCs for the detection of metal ions, rhodamine B-derived monomers were synthesized and doped into LC droplets. Theoretically, based on the radial alignment of LCs in spherical balls [25, 42], a linear segment of the synthesized rhodamine B derivatives may align with LC molecules, and a highly sterically hindered rhodamine B terminal may exist at the surface of the LC beads. Color variation in the LC beads is expected due to the surface coordination between the rhodamine B-derived dopants and metal ions leading to a chromatic reaction. To study the chromatic application of LC beads for ion detection, fabrication and optical characterization of LC beads with rhodamine B-derived monomers were carried out.

Materials and methods

Materials

All chemicals were purchased and used without any further purification. Calcium hydride (93%), CuBr (98%), potassium iodide (99.5%), azobisisobutyronitrile, and 4-dimethylamino pyridine (99%) were purchased from ACROS Chemicals, USA. Styrene (99%) and ethyl-alpha-bromoisobutyrate (97%) were purchased from Fluka, USA. 4-Hydroxycinnamic acid (98%), N,N′-dicyclohexylcarbodiimide (99%), N,N′-dimethylaniline and tris[2-(dimethylamino) ethyl]amine (Me_6TREN) (99%) were purchased from Alfa Aesar, USA. N,N,N′,N′,N″-Pentamethyldiethylenetriamine was purchased from Aldrich, USA. Solvents such as tetrahydrofuran (THF), ethyl acetate, chloroform, dichloromethane, and other solvents were purchased from Tokyo Chemical Industry, Tokyo, Japan.

Instruments

All new compounds were identified using Fourier transform infrared spectroscopy (FTIR), ^{1}H-NMR, and ^{13}C-NMR spectroscopy. FTIR spectra were recorded with a KBr disk on a Jasco VALOR III (Tokyo, Japan) FTIR spectrophotometer. ^{1}H-NMR (400 MHz) and ^{13}C-NMR (100.6 MHz) spectra were obtained on a Bruker AMX-400 (Darmstadt, Germany) high-resolution NMR spectrometer, and chemical shifts are reported in ppm relative to tetramethylsilane as an internal standard. The gel permeation chromatography measurements were performed using ViscoGEL I-Series Columns (catalog numbers: I-MBLMW-3078 and I-MBMMW-3078) of Viscotek and equipped with UV–vis and refractive index detectors. The standard was polystyrene at molecular weights of 170,000, 65,000, 25,000, 13,000, 5200, and 2200 Da. The mobile phase consisted of THF, the column temperature was maintained at 35 °C, and the flow rate was 1 ml/min. The phase transitions were investigated with an Olympus BH-2 POM equipped with a Mettler hot stage FP-82, and the temperature scanning rate was determined to be 10 K min^{-1}. Thermal decomposition temperature data were recorded under a nitrogen atmosphere at a heating rate of 20 K min^{-1} with a PerkinElmer TGA 7 for thermogravimetric analysis (TGA). UV/Vis absorption spectra were measured with a Jasco V-550 spectrophotometer.

Synthesis of precursors and final rhodamine B-derived monomer

Synthetic routes of precursors and probe molecules are shown in Schemes 1–4. The following section provides a detailed description of the experimental conditions and steps.

Synthesis of rhodamine B hydrazide (1)

Rhodamine B hydrazide (**1**) was synthesized by following reported procedures [36]. Hydrazine hydrate (18 ml, excess) was added dropwise into a 250 ml flask containing rhodamine B (4.8 g, 10 mmol) dissolved in 100 ml of ethanol, which was heated to reflux overnight. After completion of the reaction, the color of the solution changed from dark

Scheme 1 Synthetic route of rhodamine B hydrazide

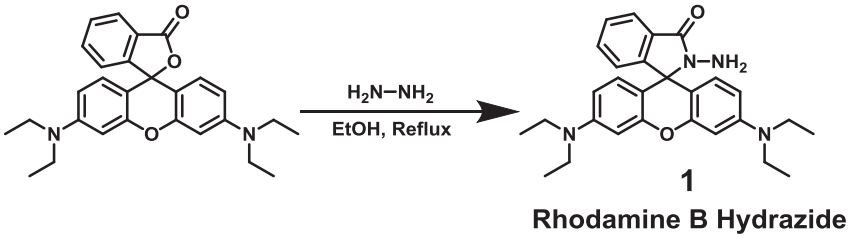

Scheme 2 Synthetic route of rhodamine B hydrazone

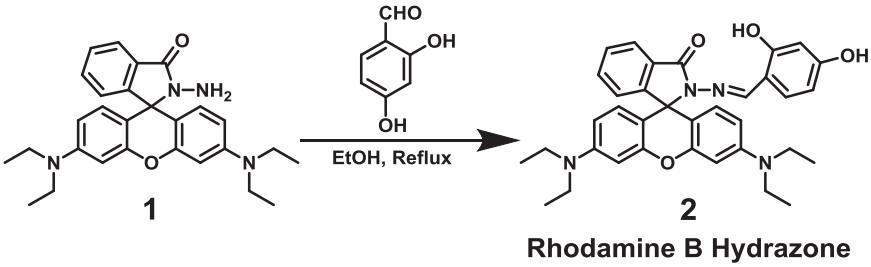

Scheme 3 Synthetic route of compound (**4**)

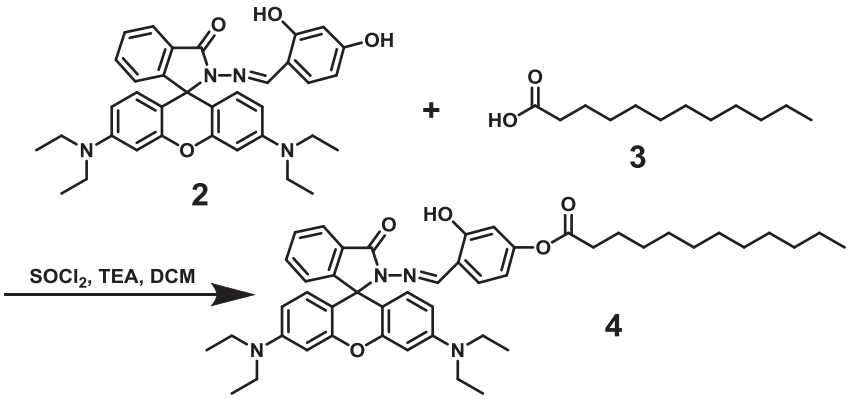

Scheme 4 Synthetic route of compound (**6**)

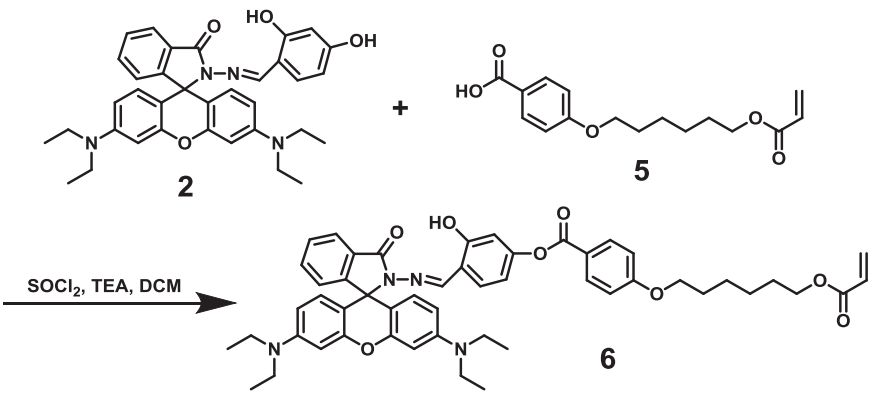

pink to transparent orange. The reaction mixture was cooled, and the solvent was removed by an evaporator. Then, 1 M $HCl_{(aq)}$ was added to the solid in a beaker to produce a clear red solution. Subsequently, 1 M $NaOH_{(aq)}$ was added slowly with stirring until the pH of the solution reached 9–10, and the product gradually precipitated and was isolated by filtration. The solid product was washed with deionized water three times and dried in an oven. In the Supplementary information, the molecular structure of the synthesized compound was identified by ^{1}H-NMR spectroscopy, as shown in Fig. S1. ^{1}H-NMR ($CDCl_3$, δ in ppm): 1.09–1.23 (t, 12H, $NCH_2\underline{CH_3}$), 3.25–3.45 (q, 8H,

NCH_2CH_3), 3.55–3.72 (s, 2H, NNH_2), 6.26–6.34 (dd, 2H, ArH), 6.38–6.52 (d, 4H, ArH), 7.04–7.15 (m, 1H, ArH), 7.37–7.52 (m, 2H, ArH), 7.88–7.98 (m, 1H, ArH).

Synthesis of rhodamine B hydrazone (2)

The synthesis of rhodamine B hydrazone (**2**) was based on a published paper [35]. Rhodamine B hydrazide (**1**) (5.7 g, 12.48 mmol) and 2,4-dihydroxybenzaldehyde (3.45 g, 24.97 mmol) were dissolved in ethanol in a 250 ml flask, and then the mixture was heated to reflux under a N_2 atmosphere overnight. The final solution was cooled and concentrated to 20 ml. After a few hours at room temperature, the precipitated crystals were filtered, washed with cold ethanol three times and dried in the oven. To identify the molecular structure, ^{1}H-NMR of the synthesized rhodamine B hydrazone (**2**) was carried out. The result is shown in Fig. S2. Each characteristic proton was confirmed as shown in the spectrum. ^{1}H-NMR ($CDCl_3$, δ in ppm): 1.12–1.19 (t, 12H, NCH_2CH_3), 3.28–3.37 (q, 8H, NCH_2CH_3), 5.0–5.21 (s, 1H, ArOH), 6.22–6.32 (m, 4H, ArH), 6.42–6.54 (d, 4H, ArH), 6.95–7.01 (d, 1H, ArH), 7.12–7.2 (d, 1H, ArH), 7.43–7.61 (m, 2H, ArH), 7.88–8.03 (d, 1H, ArH), 9.15–9.27 (s, 1H, NCH), 10.95–11.09 (s, 1H, ArOH).

Synthesis of compound (4)

Lauric acid (**3**) (60 g, 0.3 mol) was placed in a triple-necked round bottom flask under a nitrogen atmosphere. Thionyl chloride (10 ml) was injected into the flask and reacted for 1 h. And aqueous sodium hydroxide solution was connected at the outlet of the nitrogen gas to neutralize hydrochloric acid released from the reaction. After the reaction, the excess thionyl chloride was removed by a rotary evaporator at 70 °C. The as-prepared precursor (0.45 g, 2.08 mmol) was placed in a triple-necked round bottom flask under a nitrogen atmosphere again. Then, rhodamine B hydrazone (**2**) (1 g, 1.73 mmol) dissolved in dichloromethane and a small drop of triethanolamine (TEA) were added into the flask. After a few hours of reaction, the mixture was extracted with deionized water to decay dodecanoyl chloride. The solvent was removed by a rotary evaporator. The crude product was recrystallized in DCMethanol = 1:29. Pure white crystals were collected. ^{1}H-NMR ($CDCl_3$, δ in ppm): 0.85–0.90 (t, 3H, CH_3), 1.14–1.18 (t, 12H, NCH_2CH_3), 1.23–1.32 (m, 16H, CH_2), 1.67–1.73 (m, 2H, CH_2), 2.47–2.51 (t, 2H, CH_2), 3.30–3.35 (q, 8H, NCH_2CH_3), 6.24–6.28 (d, 2H, ArH), 6.45–6.49 (m, 4H, ArH), 6.5–6.54 (d, 1H, ArH), 6.56–6.59 (s, 1H, ArH), 7.05–7.10 (d, 1H, ArH), 7.16–7.20 (d, 1H, ArH), 7.48–7.56 (m, 2H, ArH), 7.95–7.99 (d, 1H, ArH), 9.15–9.18 (s, 1H, NCH), 11.05–11.07 (s, 1H, ArOH).

Synthesis of rhodamine B-derived monomer (6)

Commercially available FSLC-074 (**5**) (1 g, 3.44 mmol) was dissolved in 50 ml of anhydrous dichloromethane under a nitrogen atmosphere in a flask equipped with a condenser. Thionyl chloride (0.3 ml, 4.03 mmol) was injected into the mixture and reacted for 1 h. Then, rhodamine B hydrazone (**2**) (1.64 g, 0.31 mmol) and a small drop of TEA in 30 ml of dichloromethane were added into the mixture. After 3 h of reaction, the reaction mixture was extracted with deionized water to degrade unreacted FSLC-074 acryloyl chloride. The solvent of the collected mixture was removed by a rotary evaporator to obtain a pink solid product. The crude product was recrystallized in DCM:ethanol:water = 1:30:5 at 4 °C in a refrigerator. After two recrystallization cycles, a pure pink powder was collected. Figure S3 shows the ^{1}H-NMR of the synthesized monomer (**6**). From the molecular structure of the monomer (**6**), the long, linear terminus was expected to align with the predesign radial LCs, showing the high sterically hindered rhodamine B terminus facing out of the LC droplet during the preparation of the polymer beads. ^{1}H-NMR ($CDCl_3$, δ in ppm): 1.14–1.18 (t, 12H, NCH_2CH_3), 1.44–1.49 (m, 2H, $CH_2CH_2CH_2$), 1.50–1.55 (m, 2H, $CH_2CH_2CH_2$), 1.69–1.74 (m, 2H, $CH_2CH_2CH_2$), 1.79–1.86 (m, 2H, $CH_2CH_2CH_2$), 3.30–3.36 (q, 8H, NCH_2CH_3), 4.01–4.05 (t, 2H, $AOCH_2CH_2$), 4.15–4.20 (t, 2H, $COOCH_2CH_2$), 5.79–5.85 (d, 1H, $CHC=CH_2$), 6.07–6.16 (dd, 1H, $CHC=CH_2$), 6.24–6.30 (s + s, 2H, ArH), 6.37–6.43 (d, 1H, $CHC=CH_2$), 6.46–6.51 (d, 2H, ArH), 6.46–6.51 (d, 2H, ArH), 6.63–6.67 (d, 1H, ArH), 6.69–6.71 (s, 1H, ArH), 6.91–6.95 (d, 2H, ArH), 7.09–7.14 (d, 1H, ArH), 7.16–7.21 (d, 1H, ArH), 7.49–7.57 (m, 2H, ArH), 7.96–8.00 (d, 1H, ArH), 8.06–8.11 (d, 2H, ArH), 9.16–9.20 (s, 1H, N=CH), 11.06–11.11 (s, 1H, ArOH).

Preparation of the LC mixture

The polymeric LC beads were made from reactive mesogens, including RM257 cross-linker and RM105 monomer, and a nonreactive mesogen of 5CB and the synthesized rhodamine B-derived monomer (**6**). Scheme S4 shows the molecular structure of the compounds used in this study. The LC mixtures were prepared in various weight ratios, as shown in Table 1. For each mixture, a small amount of chloroform was used to homogeneously mix the components. After evaporation of the solvent, the LC phase was observed.

Polymerization of LC beads

The LC mixture was first injected into deionized water containing sodium dodecyl sulfate (SDS) in a glass vial

and stirred or sonicated to generate LC droplets floating in an aqueous solution. LC monomeric droplets aligned in a radial conformation due to the existence of SDS in the aqueous solution. The glass vial containing LC droplets was placed horizontally under UV light at a distance of 1 cm. The LC monomeric droplets were heated to the LC phase temperature and then exposed to 254 nm UV light for 5 h to form polymeric LC beads for further study of Cu^{2+} detection. To investigate the sensing behaviors of these reflective UV–vis probes, large size (~1 mm) LC beads were also prepared. The mixtures were first heated to fluidity, and then a fixed amount of LC mixture was injected into deionized water containing SDS.

Removal of the unreacted components

The well-polymerized LC beads were immersed in ethanol for a few hours and washed with ethanol and then deionized water three times to remove the unreacted components.

Monitoring of the sensing ability using a reflective UV–vis probe

To study the sensing ability of the fabricated LC beads via a reflective UV–vis probe, the synthesized large polymeric LC beads were placed between two parallel quartz glasses. The substrate glasses were separated by four 325 µm stacked spacers. A mirror was placed under this sample cell to reflect the UV–vis light to the probe. The schematic setup is shown in Fig. 1.

Table 1 Composition of LC mixtures (wt%)

Sample	5PA	5PB	5PC
RM257	19.04	17.62	15.26
RM105	69.28	60.62	54.27
5CB	10.64	20.8	29.47
Compound (**6**)	0.53	0.56	0.55
Irg 184	0.5	0.4	0.45

Synthesis of polymer beads without liquid crystals

For comparison, the synthesized monomeric compound (**6**) (0.6 wt%) was copolymerized with methyl methacrylate (MMA) (79 wt%) and ethylene glycol dimethacrylate (EGDMA) (20 wt%) in the presence of Irg 184 (0.5 wt%). Similar to the process of the fabrication of polymeric LC beads described in "Polymerization of LC beads", polymerization of the monomer mixture was carried out. After copolymerization, crosslinked polymer beads were obtained.

Results and discussion

Synthesis of rhodamine B derivatives

Schemes 1–4 show the synthesis of rhodamine B derivatives. The synthesized molecular structures were identified using ^{1}H-NMR. As shown in the Supplementary Information, Figs. S1–S3 show the ^{1}H-NMR spectra of the synthesized compounds. In addition, the absorption of each of the functional groups of synthesized compounds **(2)**, **(4)**, and **(6)** was further identified using FTIR.

Metal ion sensing of compound (6) via UV–Vis spectroscopy

To investigate the selectivity of compound (**6**) for specific metal ions, the sensing behavior toward different metal ions (K^+, Na^+, Ca^{2+}, Al^{3+}, Zn^{2+}, Cr^{3+}, Fe^{3+}, Pb^{2+}, Co^{2+}, Ni^{2+}, Cu^{2+}, Hg^{2+}, and Ag^+) was studied using UV–vis spectroscopy. One hundred equivalents of metal ion solution were added into a solution containing 10 µM compound in THF/H_2O (1:1 v/v). The samples were tested within 2 h after the solutions were freshly prepared at room temperature.

The UV–vis spectroscopy results of the sample ions are shown in Fig. 2a. Obvious peaks at 560 nm in Fig. 2a showing the coordination of the synthesized compounds with Cu^{2+} were found in contrast to other metal ions. In addition, the real images of the sample sensing under

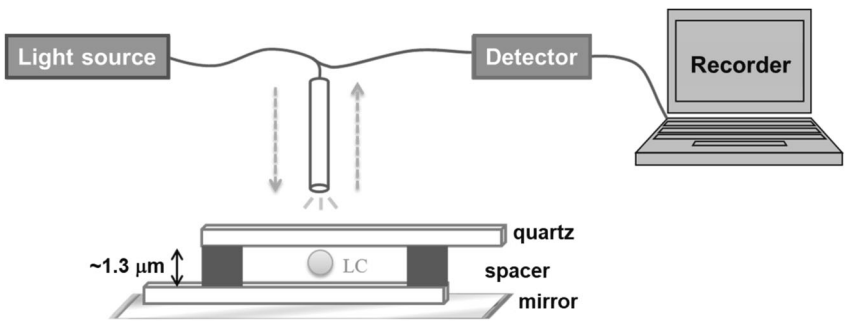

Fig. 1 A schematic setup for detection, monitoring of sensing ability using reflective UV-vis optical fiber probe

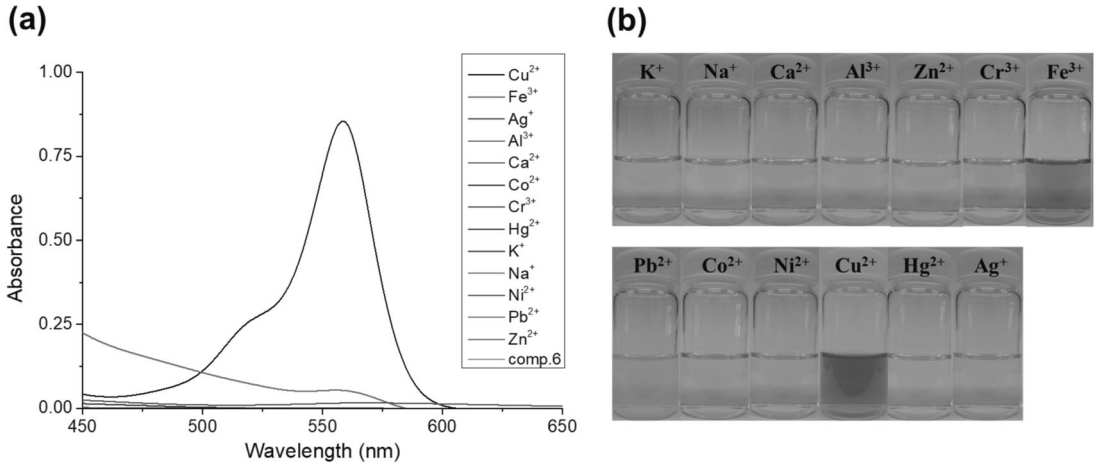

Fig. 2 Results of detection using compound (**6**), **a** UV–vis spectra and **b** real color appearance of the synthesized monomer **(6)** (10 μM) in THF/H_2O (1:1 v/v) in the presence of metal ions (1 mM, 100 equiv.)

natural light are shown in Fig. 2b. The color of the solution changed significantly from colorless to pink when the sensing probes encountered Cu^{2+}. The color change can be recognized by the naked eye, suggesting the formation of ring-open amide complexes coordinated with Cu^{2+}. The yellow color of the sample with Fe^{3+} comes from the original color of the Fe^{3+} solution. These results show the sensing selectivity of the synthesized compound toward Cu^{2+}.

Sensing mechanism of the probe with copper ions

Similar to previously published literature, the chromogenic response of probe (**6**) toward Cu^{2+} may be due to the spiro ring-opening mechanism [43]. When the structure of the synthesized compound displays a spirocyclic form, it is colorless. In contrast, the coordination of compound (**6**) with Cu^{2+} leads to the ring-opening reaction resulting in the pink color. Figure S5 shows the sensing mechanism of the probe molecule (**6**) with copper ions.

Molecular alignment of LC droplets

To fabricate stable, recyclable, and selective LC beads for sensing, polymeric LC beads were prepared using reactive mesogens of RM257 and RM105, a nonreactive mesogen of 5CB and a rhodamine B-derived monomer. The rhodamine B-derived compound (**6**) is capable of detecting Cu^{2+}. First, LC monomeric droplets were aligned in a radial conformation by immersing the LC droplets in an aqueous SDS solution. The LC monomeric droplets were then UV-polymerized to form polymeric LC beads for further study of Cu^{2+} detection.

As noted in the literature, adding SDS to nonionic surfactants results in the radial arrangement of LC droplets in deionized water [36, 37]. Figure 3a, b shows the POM texture of pure 5CB droplets and **5PA** LC sample droplets in SDS-added DI water. The results suggest that both droplets in SDS-containing DI water are arranged in the same radial alignment. As shown in Fig. S6, the radial LC droplet shows similar POM textures as reported. Figure 3c shows a schematic representation of the radially aligned LC molecules. As shown in Fig. 3d, the linear terminal of monomer (**6**) may align with LCs, leaving a highly sterically hindered spirocyclic terminal outside the LC droplet. Figure 3d enlarged image shows the internal molecular alignment and surfactant-like interaction of monomer (**6**) at the droplet surface. From the reported literature [44], spherical LC droplets exhibiting solution-induced perpendicular anchoring will form an internal radial direction conformation and reveal a bright-fan-shaped pattern under POM observation.

It is expected that the molecular arrangement of the LC droplet aligns in a radial conformation, and the long carbon chain of compound (**6**) may insert into the alignment of 5CB to expose the coordination group outside of the droplet. The surfactant SDS is usually used to increase homeotropic anchoring at the interface between the aqueous solution and LC droplets due to molecular interactions. The LC droplets were dispersed in 0.1 wt% SDS aqueous solution by sonication and then exposed to UV light (254 nm). After photopolymerization, the arrangement of the LC molecules was maintained, which was confirmed by the POM images.

For the relatively high concentration of 5CB, namely, that of samples **5PB** and **5PC**, obvious bright-fan-shaped patterns were observed, showing the preservation of the radial conformation of LC molecules before and after polymerization, as shown in Fig. S7(ii), (iii). In contrast, uncharacteristic patterns of sample **5PA**, namely, the low concentration of 5CB in the LC droplets, were observed before and after polymerization, as shown in Fig. S7(i). This result could be because a decrease in 5CB drastically

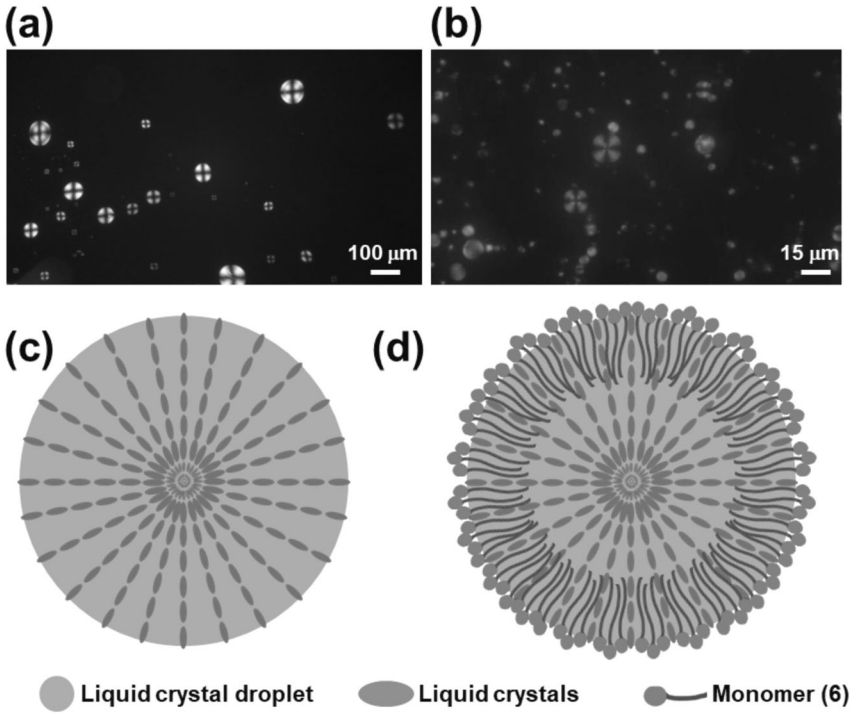

Fig. 3 Radial arrangement of LC droplet, POM image of **a** a pure 5CB droplet, **b** a **5PA** liquid crystal sample droplet, **c** schematic presentation of radial liquid crystal alignment, and **d** monomer (**6**) aligned at the LC droplet surface

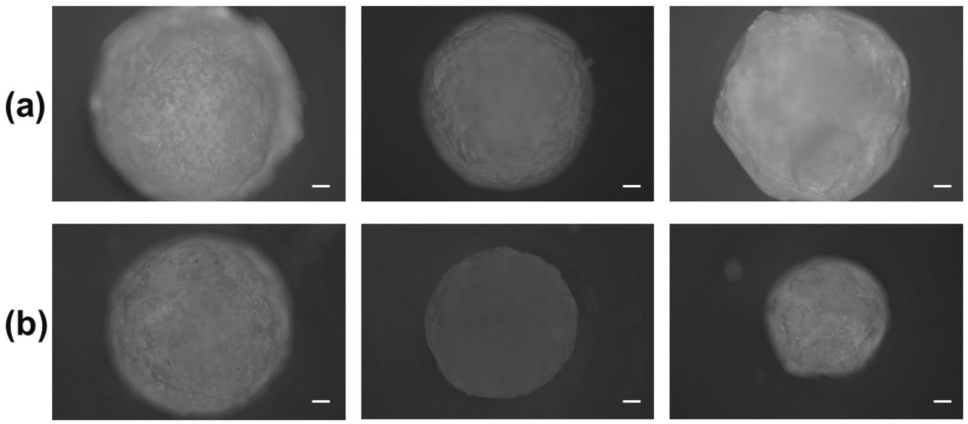

Fig. 4 Morphology of LC beads, optical microscope (OM) images of the synthesized (i) **5PA**, (ii) **5PB**, and (iii) **5PC** beads (**a**) before and (**b**) after extraction with ethanol. Scale bars indicate 100 μm

decreased the coordinating sites at the surface, leading to a weakening of the directing ability.

It is noteworthy that polymeric LC beads revealed a deep pink color after UV polymerization due to the UV-induced ring-opening reaction. After keeping the beads in the dark for 1 day, a ring-closure reaction occurred, leading to the beads changing to light pink. A similar reversible photochromic phenomenon was mentioned in a published paper [24–27].

To investigate the sensing behaviors of reflective UV–vis probes, larger LC beads were prepared. Accordingly, it was difficult to observe the specific patterns under the monitoring of POM. As shown in Fig. 4a, a rough surface of the bead was observed. After removing unreacted LC compounds, the synthesized beads should be porous. To remove unreacted chemicals, the fabricated beads were washed with ethanol a few times. Figure 4a, b shows the polymeric LC beads before and after washing with ethanol, respectively. After washing, the beads were reduced to sizes smaller than the original beads, but the spherical shape was maintained.

Detection of metal ions using polymeric LC beads

The detailed components of **5PA**, **5PB**, and **5PC** are shown in Table 1. The sample beads contain almost the same amount of sensing compound (**6**). 5CB is a non-reactive LC. However, an increase in 5CB shows a high

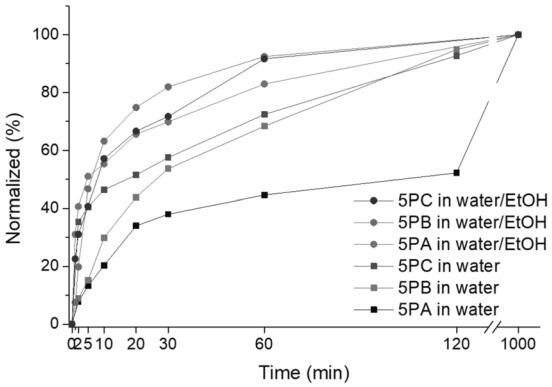

Fig. 5 Sensing ability of sample beads, normalized comparison of the sensing rate between different compositions of LC beads with or without ethanol in the system

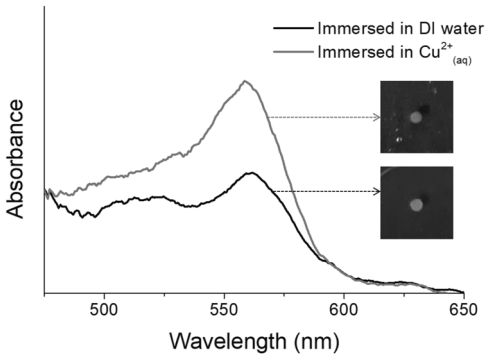

Fig. 6 Detection of copper ions via sample beads, UV–vis spectra of the detection of 5×10^{-6} M Cu^{2+} in DI water/ethanol (1:1 v/v) solution using **5PC** polymeric LC beads

radial arrangement of molecules. After polymerization, removing 5CB forms the porous structure of polymer beads, leading to an increase in the metal ion sensing ability. To study the effect of nonreactive mesogen 5CB on the sensing ability, polymeric LC beads were made in millimeter sizes. For such synthesized beads, the absorption band could be monitored by reflective UV–vis spectrometry. The beads were immersed in solution and placed between two parallel quartz slides to reduce scattering. Figure S8 shows the results for the sensing rate of the synthesized LC beads in 10^{-3} M Cu^{2+} aqueous solution. Over time, the intensity of the absorbance increased for all the samples, indicating that the coordination reaction occurred gradually. For comparison, the intensity of the absorbance was normalized to the peak at 560 nm, and the function is shown below:

$$\text{Normalized}\,(\%) = \frac{I - I_{0\,\text{min}}}{I_{\text{infinite}} - I_{0\,\text{min}}}, \qquad (1)$$

where I is the intensity of absorbance at each time; $I_{0\,\text{min}}$ is the intensity of absorbance before adding Cu^{2+} aqueous solution; and I_{infinite} is the intensity of absorbance for infinite time.

The sensing rates of (i) **5PA**, (ii) **5PB**, and (iii) **5PC** polymeric LC beads in (a) 10^{-3} M Cu^{2+} aqueous solution and (b) 10^{-3} M Cu^{2+} DI water/ethanol (1:1 v/v) solution under reflective UV–vis monitoring are shown in Fig. S8. From Fig. S8, the normalized results of each case are summarized in Fig. 5. The results indicate that increasing the concentration of 5CB increased the sensing rate of the beads. Sample **5PA** containing 10 wt% 5CB shows only a low sensing efficiency. This result is ascribed to the low pore density of the beads, leading to difficult diffusion of the copper ions to coordinate with compound (**6**). As shown in Fig. 5, both sample **5PB** and **5PC** reached 90% of the infinite time intensity in 2 h. Sample **5PC** could even reach the maximum absorbance intensity in a few minutes; to be more specific, the color change from light pink to dark pink could be distinguished by the naked eye quickly and easily.

To facilitate the sensing properties, the polymeric LC beads were immersed in a 10^{-3} M Cu^{2+} DI water/ethanol (1:1 v/v) solution. Although different pore size beads exhibited different diffusion rates for the Cu^{2+} aqueous solution, this phenomenon was diminished by the introduction of ethanol, causing a decrease in the surface tension. A significant signal increase was observed within the initial 5 min for all samples.

To use a UV–vis probe for detection, a confined sample cell was used. Due to the surface interaction from the cell substrates, the fluidity of the solution between the slides was limited, leading to a decrease in the sensing rate. To demonstrate this effect, the synthesized beads were placed in a glass vial. In this case, an obvious color change was observed 2 min after adding the eCu^{2+} aqueous solution with continuous shaking of the vial.

Detection of low-concentration Cu^{2+} via LC beads

To study the low concentration of Cu^{2+} using polymeric LC beads, beads with large sizes were immersed into the sample solution, placed between two parallel quartz slides and monitored using a reflective UV–vis probe. When the sample **5PC** LC beads were immersed in deionized water, a peak at 560 nm was found in the absorption spectrum, indicating the light pink color of LC beads, as shown in Fig. 6. After the removal of deionized water from the sample cell, the solution containing 5×10^{-6} M Cu^{2+} DI water/ethanol (1:1 v/v) was filled into the system. However, the color of LC beads could be observed by the naked eye several hours after the addition of copper ions. The intensity of the absorbance increased gradually, indicating coordination between rhodamine and Cu^{2+}.

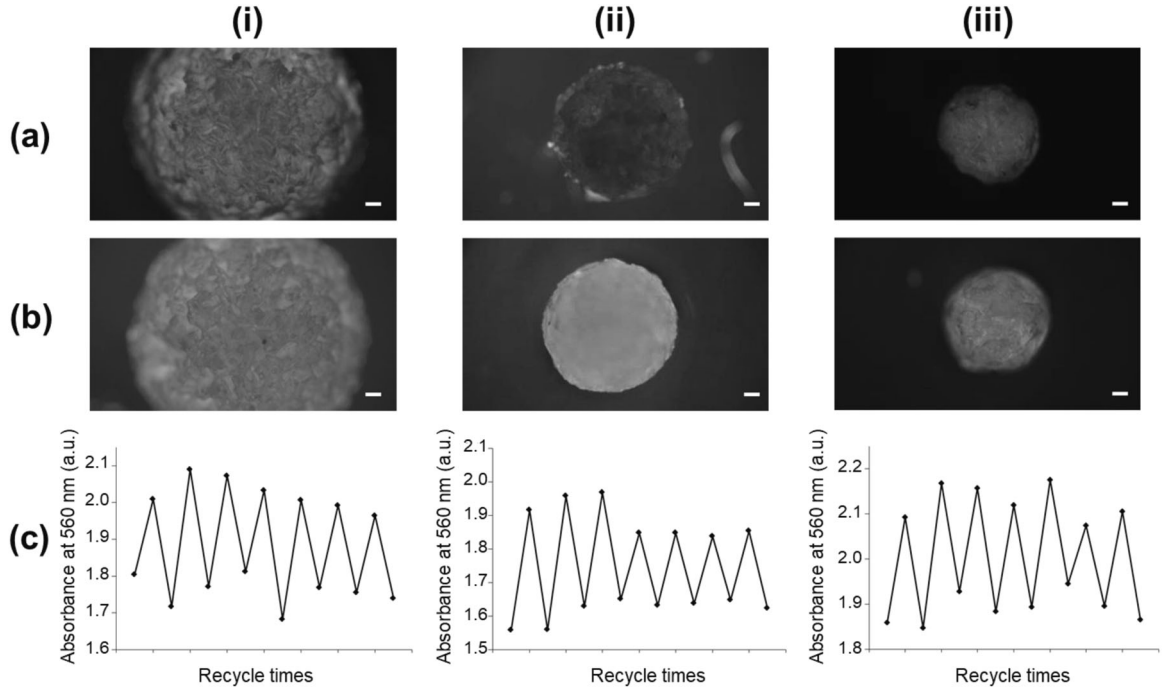

Fig. 7 Detection stability of sample beads, recyclable behaviors of (i) **5PA**, (ii) **5PB**, and (iii) **5PC** beads under monitoring of OM when (**a**) exposed to $Cu^{2+}{}_{(aq)}$ and (**b**) washed by $NH_4OH_{(aq)}$, and (**c**) under monitoring of reflective UV–vis. Scale bars indicate 100 μm

After the LC beads were kept in 5×10^{-6} M Cu^{2+} DI water/ethanol (1:1 v/v) solution for 1 day, the dark pink color of the beads was observed.

Recyclable polymeric LC beads

After sensing, the synthesized polymeric LC beads were recovered by adding aqueous ammonia. This behavior is beneficial for use as a sensor. Figure 7 reveals the recyclable behaviors of the LC beads monitored using POM. After sensing, the beads were coordinated with copper ions, showing a dark pink color, as shown in Fig. 7a. Once aqueous ammonia was added into the sensing system, the copper ions were removed from the beads by ammonia immediately, resulting in a light pink color, as shown in Fig. 7b. The chelating power between copper ions and ammonia is greater than that between copper ions and the coordinating group of compound (**6**).

To monitor the recyclable behavior using a reflective UV–vis probe, the beads were immersed in a solution and placed between confined quartz slides again. The intensity of the absorbance at 560 nm of the samples is summarized in Fig. 7c. Each of the synthesized samples could be recycled at least eight times. However, as the number of recycling cycles increased, the detection sensitivity gradually decreased. The sensing ability of a significant color change was maintained.

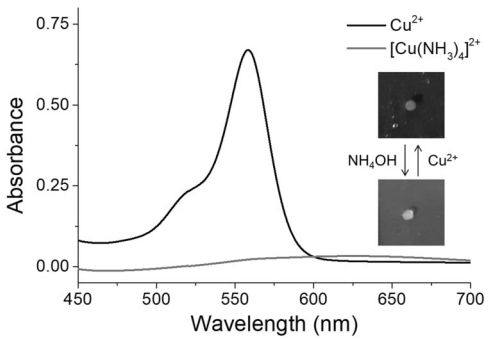

Fig. 8 Reversibility of compound (**6**), UV–vis spectra of recyclable ion detection of compound (**6**). (10 μM compound (**6**) was added to 10 μM Cu^{2+} in THF/H_2O (1:1 v/v) and recovered by NH_4OH)

Reversibility of synthesized compound (6)

To confirm the reversibility of synthesized compound (**6**), the UV–vis absorption of compound (**6**)-Cu^{2+} complexes (10 μM compound (**6**) with 10 μM Cu^{2+}) in THF/H_2O (1:1 v/v) before and after the addition of aqueous ammonia was studied. The results are shown in Fig. 8. In the UV–vis absorption spectra, a strong absorption peak at 560 nm was observed due to the formation of compound (**6**)-Cu^{2+} complexes. However, the absorption peak disappeared when aqueous ammonia was added. In the real images, the color changed from dark pink to colorless before and after the addition of aqueous ammonia, respectively. The

phenomenon could be easily recognized by the naked eye. The appearance of color is ascribed to the formation of $[Cu(NH_3)_4]^{2+}$, leading to the ring-closure reaction of compound (**6**). The $[Cu(NH_3)_4]^{2+}$ complex reveals a deep blue color, but the amount of the complex was too low to be detected by UV–vis spectroscopy.

Fabrication of polymer beads without liquid crystal assistance

For comparison, the synthesized compound (**6**) was mixed with regular monomeric MMA and EGDMA without any LC assistance. After polymerization of the monomer mixture, crosslinked polymer beads were obtained. However, the synthesized polymer beads did not show any sensing ability. The results suggest that without the assistance of LCs, after polymerization, compound (**6**) monomers were blocked inside the polymer beads, leading to the disappearance of the sensing properties.

Conclusion

To detect specific metal ions, a sensing probe molecule derived from rhodamine B was synthesized. From the results of the UV–vis analysis, the selective sensing of Cu^{2+} via the synthesized rhodamine derivative was confirmed. The synthesized rhodamine derivatives were homogeneously mixed with LC-forming beads. A study on the selective detection of Cu^{2+} via the synthesized rhodamine derivatives aligned with LCs was carried out.

Recyclable polymeric LC beads were prepared from reactive mesogens of RM257 and RM105, a nonreactive mesogen of 5CB and a rhodamine-derived compound (**6**). The color of the polymeric LC beads changed from light pink to deep pink after dropping the LC beads into a Cu^{2+} aqueous sample solution. Different detection rates of the beads were observed depending on the distinct pore density caused by various amounts of 5CB. A low concentration of 5×10^{-6} M Cu^{2+} in DI water/ethanol (1:1 v/v) solution was detected using the synthesized LC beads. The beads were recovered by adding aqueous ammonia due to the formation of $[Cu(NH_3)_4]^{2+}$. Each of the synthesized LC probe beads could be recycled at least eight times. The fabricated LC beads possess high sensitivity to copper ions in aqueous solution and will be suitable for engineering and environmental applications.

Acknowledgements The authors would like to thank the Ministry of Science and Technology (MOST) of the Republic of China (Taiwan) for financially supporting this research under contract MOST 107-2923-E-006-001 and MOST 108-2218-E-006-049. This research was also supported in part by the Higher Education Sprout Project, Ministry of Education to the Headquarters of University Advancement at National Cheng Kung University (NCKU).

Compliance with ethical standards

Conflict of interest The authors declare that they have no conflict of interest.

Publisher's note Springer Nature remains neutral with regard to jurisdictional claims in published maps and institutional affiliations.

References

1. Jiao Z, Zhang P, Chen H, Li C, Chen L, Fan H, et al. Differentiation of heavy metal ions by fluorescent quantum dot sensor array in complicated samples. Sens Actuators B Chem. 2019;295:110–6.
2. Araoka F, Shin KC, Takanishi Y, Ishikawa K, Takezoe H, Zhu Z, et al. How doping a cholesteric liquid crystal with polymeric dye improves an order parameter and makes possible low threshold lasing. J Appl Phys. 2003;94:279–83.
3. Raghunandhan R, Chen LH, Long HY, Leam LL, So PL, Ning X, et al. Chitosan/PAA based fiber-optic interferometric sensor for heavy metal ions detection. Sens Actuators B Chem. 2016;233:31–8.
4. Denis M, Pancholi J, Jobe K, Watkinson M, Goldup SM. Chelating rotaxane ligands as fluorescent sensors for metal ions. Angew Chem Int Ed. 2018;57:5310–4.
5. Lee SJ, Lee JE, Seo J, Jeong IY, Lee SS, Jung JH. Optical sensor based on nanomaterial for the selective detection of toxic metal ions. Adv Funct Mater. 2007;17:3441–6.
6. Molina P, Tárraga A, Caballero A. Ferrocene-based small molecules for multichannel molecular recognition of cations and anions. Eur J Inorg Chem. 2008;2008:3401–17.
7. Sugunan A, Thanachayanont C, Dutta J, Hilborn JG. Heavy-metal ion sensors using chitosan-capped gold nanoparticles. Sci Tech Adv Mater. 2005;6:335–40.
8. Harzat A, Ezzat K, Ikram I. Environmental chemistry and ecotoxicology of hazardous heavy metals: environmental persistence, toxicity, and bioaccumulation. J Chem. 2019;2019:6730305.
9. Mehrandish R, Rahimian A, Shahriary A. Heavy metals detoxification: a review of herbal compounds for chelation therapy in heavy metals toxicity. J Herbmed Pharm. 2019;8:69–77.
10. Baatrup E. Structural and functional effects of heavy metals on the nervous system, including sense organs, of fish. Comp Biochem Physiol. 1991;100:253–7.
11. Bost M, Houdart S, Oberli M, Kalonji E, Huneau JF, Margaritits I. Dietary copper and human health: current evidence and unresolved issues. J Trace Elem Med Biol. 2016;35:107–15.
12. Gaetke LM, Chow-Johnson HS, Chow CK. Copper: toxicological relevance and mechanisms. Arch Toxicol. 2014;88:1929–38.
13. Valfredo AL, Elenir SS, Ednilton MG. A comparative study of two sorbents for copper in a flow injection preconcentration system. Sep Purif Technol. 2007;56:212–9.
14. Santos EM, Ball JS, Williams TD, Wu H, Ortega F, Aerle RV, et al. Identifying health impacts of exposure to copper using transcriptomics and metabolomics in a dish model. Environ Sci Technol. 2010;44:820–6.
15. Skibniewski M, Skibniewska EM, Kosia T, Olbrych K. The content of copper and molybdenum in the liver, kidneys, and skeletal muscles of elk (*Alces alces*) from North-Eastern Poland. Biol Trace Elem Res. 2016;169:204–10.
16. Marwa AI, Mai DI. Acrylamide-induced hematotoxicity, oxidative stress, and DNA damage in liver, kidney, and brain of catfish (*Clarias gariepinus*). Environ Toxicol. 2020;35:300–8.
17. Li Q, Liu H, Alattar M, Jiang S, Han J, Ma Y. et al. The preferential accumulation of heavy metals in different tissues

following frequent respiratory exposure to $PM_{2.5}$ in rats. Sci Rep.2015;5:16936.
18. Iamsaard S, Anger E, Aßhoff SJ, Depauw A, Fletcher SP, Katsonis N. Fluorinated azobenzenes for shape-persistent liquid crystal polymer networks. Angew Chem Int Ed. 2016;55: 9908–12.
19. Keith JM, King JA, Miller MG, Tomson AM. Thermal conductivity of carbon fiber/liquid crystal polymer composites. J Appl Poly Sci. 2006;102:5456–62.
20. Cattle J, Bao P, Bramble JP, Bushby RJ, Evans SD, Lydon JE, et al. Controlled planar alignment of discotic liquid crystals in microchannels made using SU8 photoresist. Adv Funct Mater. 2013;23:5997–6006.
21. Serra F, Eaton SM, Cerbino R, Buscaglia M, Cerullo G, Osellame R, et al. Nematic liquid crystals embedded in cubic microlattices: memory effects and bistable pixels. Adv Funct Mater. 2013;23: 3990–4.
22. Yu H, Szilvási T, Rai P, Twieg RJ, Mavrikakis M, Abbott NL. Computational chemistry-guided design of selective chemoresponsive liquid crystals using pyridine and pyrimidine functional groups. Adv Funct Mater. 2018;28:1703581.
23. Bögels GM, Lugger JAM, Goor OJGM, Sijbesma RP. Size-selective binding of sodium and potassium ions in nanoporous thin films of polymerized liquid crystals. Adv Funct Mater. 2016;26:8023–30.
24. Jung YD, Khan M, Park SY. Fabrication of temperature- and pH-sensitive liquid-crystal droplets with PNIPAM-*b*-LCP and SDS coatings by microfluidics. J Mater Chem B. 2014;2:4922–8.
25. Wang N, Evans JS, Liu Q, Wang S, Khoo IC, He S. Electrically controllable self-assembly for radial alignment of gold nanorods in liquid crystal droplets. Opt Mat Express. 2015;5:1065–70.
26. Lee JH, Kamel T, Roth SV, Zhang P, Park SY. Structures and alignment of anisotropic liquid crystal particles in a liquid crystal cell. RSC Adv. 2014;4:40617.
27. Wang Y, Chang H, Wu W, Peng W, Yan Y, He C, et al. Rhodamine 6 G hydrazone bearing pyrrole unit: ratiometric and selective fluorescent sensor for Cu^{2+} based on two different approaches. Sens Actuators B Chem. 2016;228:395–400.
28. Doumani N, Maroun EB, Maalouly J, Tueni M, Dubois A, Bernhard C, et al. A new pH-dependent macrocyclic rhodamine B-based fluorescent probe for copper detection in white wine. Sensors. 2019;19:4514.
29. Maji A, Lohar S, Pal S, Chattopadhyay P. A New rhodamine based 'turn-on' Cu^{2+} ion selective chemosensor in aqueous system applicable in bioimaging. J Chem Sci. 2017;129: 1423–30.
30. Li XM, Zhao R, Yang Y, Lv XW, Wei YL, Tan R, et al. A Rhodamine-based fluorescent sensor for chromium ions and its application in bioimaging. Chin Chem Lett. 2017;28:1258–61.
31. Wang J, Long L, Xiao G, Fang F. Reversible fluorescent turn-on sensors for Fe^{3+} based on a receptor composed of tri-oxygen atoms of amide groups in water. Open Chem. 2018;16:1268–74.
32. Cui P, Jiang X, Sun J, Zhang Q, Gao F. A water-soluble rhodamine B-derived fluorescent probe for pH monitoring and imaging in acidic regions. Methods Appl Fluoresc. 2017;5:024009.
33. Singh SK, Nandi R, Mishra K, Singh HK, Singh RK, Singh B. Liquid crystal based sensor system for the real time detection of mercuric ions in water using amphiphilic dithiocarbamate. Sens Actuators B Chem. 2016;226:381–7.
34. Han GR, Jang CH. Detection of heavy-metal ions using liquid crystal droplet patterns modulated by interaction between negatively charged carboxylate and heavy-metal cations. Talanta. 2014;128:44–50.
35. Xu Z, Zhang L, Guo R, Xiang T, Wu C, Zheng Z, et al. A highly sensitive and selective colorimetric and off–on fluorescent chemosensor for Cu^{2+} based on rhodamine B derivative. Sens Actuators B Chem. 2011;156:546–52.
36. Xu L, Xu Y, Zhu W, Zeng B, Yang C, Wu B, et al. Versatile trifunctional chemosensor of rhodamine derivative for Zn^{2+}, Cu^{2+} and His/Cys in aqueous solution and living cell. Org Biomol Chem. 2011;9:8284–7.
37. Jun Y, Péter S, Daniel AP, John MDS, Corrie TI, Antal J, et al. Spherical-cap droplets of a photo-responsive bent liquid crystal dimer. Soft Matter. 2019;15:989–98.
38. Poon CK, Tang O, Chen XM, Kim B, Hartlieb M, Pollock CA. et al. Fluorescent labeling and biodistribution of latex nanoparticles formed by surfactant-free RAFT emulsion polymerization. Macromol Biosci. 2017;17:1600366.
39. Kumar D, Talreja N. Nickel nanoparticles-doped rhodamine grafted carbon nanofibers as colorimetric probe: naked eye detection and highly sensitive measurement of aqueous Cr^{3+} and Pb^{2+}. Korean J Chem Eng. 2019;36:126–35.
40. Tseng MH, Hu CC, Chiu TC. A fluorescence turn-on probe for sensing thiodicarb using rhodamine B functionalized gold nanoparticles. Dyes Pigm. 2019;171:107674.
41. Saha S, Chhatbar MU, Mahato P, Praveen L, Siddhanta AK, Das A. Rhodamine–alginate conjugate as self indicating gel beads for efficient detection and scavenging of Hg^{2+} and Cr^{3+} in aqueous media. Chem Commun. 2012;48:1659–61.
42. Wnag D, Park SY, Kang IK. Liquid crystals: emerging materials for use in real-time detection applications. J Mater Chem C. 2015;3:9038–47.
43. Kim HN, Lee MH, Kim HJ, Kim JS, Yoon J. A new trend in rhodamine-based chemosensors: application of spirolactam ring-opening to sensing ions. Chem Soc Rev. 2008;37:1465–72.
44. Niu X, Luo D, Chen R, Wang F. Optical biosensor based on liquid crystal droplets for detection of cholic acid. Opt Commun. 2016;381:286–91.